cGAS–STING Pathway Activation during *Trypanosoma cruzi* Infection Leads to Tissue-Dependent Parasite Control

Natasha Perumal,*,† Brooke White,* Fernando Sanchez-Valdez,* and Rick L. Tarleton*,†

Host cell invasion by *Trypanosoma cruzi* is a markedly silent process, with limited host transcriptional changes indicative of innate immune recognition, except for a modest type I IFN (IFN-I) response. In this study, we show that *T. cruzi*–induced IFN-β production was nearly abolished in primary murine cGAS$^{-/-}$ or stimulator of IFN genes (STING)-deficient (STING^{Gt}) macrophages and fibroblasts. *T. cruzi* infection did not impact the ability of IFN-regulatory factor reporter macrophages to respond to classical cGAS–STING agonists, indicating that the limited IFN-β induction is not due to active parasite suppression. cGAS$^{-/-}$, STING^{Gt}, and IFN-α/β receptor$^{-/-}$ (IFNAR$^{-/-}$) macrophages infected with *T. cruzi* yielded significantly higher numbers of amastigotes compared with wild-type macrophages; however, the impact of the STING pathway during infection in vivo is more complex. Despite an initial increase in parasite growth, STING^{Gt} and IFNAR$^{-/-}$ mice ultimately had lower parasite burden in footpads as compared with wild-type mice, demonstrating a role for IFN-I expression in potentiating parasite growth at the infection site. STING pathway activation had little impact on parasite levels in the skeletal muscle; however, in the heart, cGAS$^{-/-}$ and STING^{Gt} mice, but not IFNAR$^{-/-}$ mice, accumulated higher acute parasite loads, suggesting a protective role of STING sensing of *T. cruzi* in this organ that was independent of IFN-I. Together, these results demonstrate that host cGAS–STING senses *T. cruzi* infection, enhancing parasite growth at the site of entry, and contributes to acute-phase parasite restriction in the heart, a major site of tissue damage in chronic *T. cruzi* infection. *The Journal of Immunology*, 2023, 211: 1–11.

The initial events of host detection of a pathogen determine the quality of innate immune defenses and provide crucial signals in shaping the subsequent adaptive immune responses (1). These events are a consequence of host cell detection of pathogen-associated molecular patterns (PAMPs) of invading pathogens by various cell-surface, vacuolar, and cytosolic pattern recognition receptors (PRRs) and pathogen-driven measures that counteract responses detrimental to their survival. Some of the earliest host–pathogen interactions that occur even before the generation of pathogen-specific immunity dictate the outcome of infection whether it be pathogen clearance or establishment of persistent infection (2–8). A better understanding of how immunological events resulting from pathogen detection potentially affect the establishment of infection has important therapeutic implications for persistent infections that remain major public health concerns (9, 10).

With respect to intracellular pathogens, infection of host cells consistently elicits a relatively rapid induction of host cell gene expression indicative of host cell PRR engagement, usually within minutes to hours of cell invasion (11). Host cell response to invasion by the protozoan pathogen *T. cruzi,* the causative agent of Chagas disease, is rather immunologically "silent" in comparison with many other pathogens, representing a potential mechanism that favors its life-long persistence in most hosts (12–15). Transcriptome analysis of *T. cruzi*–infected cells shows minimal induction of proinflammatory cytokines throughout the invasion process both in vitro and in vivo at the site of infection (16, 17). Although various *T. cruzi* PAMPs have been characterized, the cell-invasive trypomastigote form appears to lack potent PAMPs exposed on its surface, likely explaining the weak host response to trypomastigote invasion (18–21). This stealth invasion can lead to the limited ability of hosts to rapidly detect and mount immune responses to new *T. cruzi* infections, or infections at new sites in an already infected host, thus likely impeding control of existing infections or resistance to reinfection, and thus the potential for vaccines to induce protection (15, 22).

Despite the lack of a strong proinflammatory response to host cell invasion, *T. cruzi* infection reproducibly elicits a modest type I IFN (IFN-I) response, which is reflected as the most notable change in host transcriptional activity at 24 h postinfection (hpi) both in vitro in immune and non-immune cells and in vivo at the site of intradermal infection (16, 17). It has been previously demonstrated that the IFN-I response to *T. cruzi* infection is generated independently of MyD88, TIR-domain-containing adapter-inducing IFN-β, and mitochondrial antiviral-signaling protein signaling, which together encompasses signaling via known cell-surface and endosomal TLRs, and intracellular dsRNA sensing machinery (23). However, it was only recently shown that the stimulator of IFN genes (STING) pathway, a key mechanism for cytosolic DNA sensing, is involved in generating the *T. cruzi*–elicited IFN-I response in an TBK1 and IFN-regulatory factor (IRF) 3–dependent manner (23, 24). In addition, transfected *T. cruzi* DNA can stimulate STING in IRF reporter cells (24), yet

*Center for Tropical and Emerging Global Diseases, University of Georgia, Athens, GA; and †Department of Cellular Biology, University of Georgia, Athens, GA

ORCIDs: 0000-0002-9693-1103 (N.P.); 0000-0002-0441-1355 (B.W.); 0000-0002-9589-5243 (R.L.T.).

Received for publication May 31, 2023. Accepted for publication July 31, 2023.

This work was supported by the National Institute of Allergy and Infectious Diseases, National Institutes of Health Grants R01AI124692 and R01AI151148. The funder had no role in the design and conduct of the study, in the collection, analysis, and interpretation of the data, and in the preparation, review, or approval of the manuscript.

Address correspondence and reprint requests to Rick L. Tarleton, University of Georgia, Coverdell Center for Biomedical Research, 500 DW Brooks Drive, Athens, GA 30602. E-mail address: tarleton@uga.edu

The online version of this article contains supplemental material.

Abbreviations used in this article: B6, C57BL/6; BMDM, bone marrow–derived macrophage; dpi, days postinfection; hpi, hours postinfection; IFNAR, IFN-α/β receptor; IFNAR1, IFN-α/β receptor subunit 1; IFN-I, type I IFN; IRF, IFN-regulatory factor; ISG, IFN-stimulated gene; kDNA, kinetoplast DNA; poly(I:C), polyinosinic-polycytidylic acid; PAMP, pathogen-associated molecular pattern; pen/strep, penicillin-streptomycin; PRR, pattern recognition receptor; STING, stimulator of IFN genes; STING^{Gt}, stimulator of IFN genes–deficient; THF, telomerase-immortalized human fibroblasts; UGA, University of Georgia; WT, wild-type.

Copyright © 2023 by The American Association of Immunologists, Inc. 0022-1767/23/$37.50

the relevant *T. cruzi* stimulus that activates STING in vivo has not been identified to date. We have recently observed that after *T. cruzi* invasion of some host cells, an asymmetric division of the trypomastigote results in the release of the parasite flagellum and its associated kinetoplast DNA (kDNA), the DNA of the single parasite mitochondrion, into the host cell cytoplasm (25). This released kDNA is potentially accessible to host cytosolic DNA sensors such as cGAS, which could drive the STING-dependent, IFN-I response in some *T. cruzi*–infected host cells (26). In addition to the well-characterized induction of IFN-I, increasing evidence reveals other functions of cGAS–STING activation during infection, including the induction of autophagy in myeloid cells, contributing to the sequestration and clearance of DNA and cytosolic pathogens (27, 28).

The STING pathway is activated by a wide range of pathogens with contrasting outcomes for the host. Activation of the STING pathway has been shown to favor effective immune responses against both DNA and RNA viruses (29–31), and its role in bacterial infections is reported to be either protective or detrimental depending on the infection (32–35). Concerning protozoan pathogens, the exposure of dead parasite genomic DNA is thought to trigger the cGAS–STING pathway in *Plasmodium* and *Toxoplasma* infections and to play a role in host defense (36–39). Recently, cytosolic delivery of purified kDNA into THP-1 macrophages infected with *Leishmania major* was demonstrated to increase parasite numbers in macrophages, implying a potential mechanism of parasite modulation of the host cGAS–STING pathway for their benefit (40).

It was recently reported that *T. cruzi*–infected mice deficient in STING have increased parasite numbers in mouse cardiac tissue (24). However, apart from this study, the role of the cGAS–STING pathway in the detection of *T. cruzi* infection in other relevant sites of infection in vivo and its potential impact in dictating the overall outcome of infection remain largely undefined. Therefore, in this study, we assessed the involvement of cGAS in the induction of IFN-I in *T. cruzi* infection via STING, and we observed distinct consequences of the STING pathway in the restriction of tissue parasite loads within tissues relevant to infection.

Materials and Methods

Mice, parasites, and infections

C57BL/6N mice were purchased from Charles River Laboratories. IFN-α/β receptor subunit $1^{-/-}$ ($IFNAR1^{-/-}$) mice were a gift from B. He (University of Georgia [UGA]) and were originally purchased from The Jackson Laboratory (Bar Harbor, ME). Goldenticket ($Tmem173^{Gt}$; C57BL/6J-Sting1gt/J) mice and cGAS $^{-/-}$ [Cgastm1d(EUCOMM)Hmgu] mice were purchased from Jackson Laboratory. $cGAS^{-/-}$ mice were crossed with STING-deficient ($STING^{Gt}$) mice and $IFNAR1^{-/-}$ mice to generate $cGAS^{-/-}STING^{Gt}$ and $cGAS^{-/-}IFNAR1^{-/-}$ mice, respectively. All mice used in experiments were sex and age matched. Mice were maintained in the UGA Animal Facility under specific pathogen-free conditions. All animal use was performed following the protocol approved by the UGA Institutional Animal Care and Use Committee.

For *T. cruzi* infections, mice were infected with tissue culture trypomastigotes of CL, Colombiana, or Brazil strains. Parasites were maintained in culture using serial passage through Vero cells. Florescent or luciferase-expressing parasites were generated by transfection with a pTREX-plasmid containing tdTomato and red-shifted firefly luciferase (41). Brazil A4 strain parasites expressing mNeon green in the nucleus (H3-mNeon Green) were generated by the expression of *T. cruzi* Histone 3 (TcCLB.509471.59) in fusion with the mNeon green gene.

Cell culture

Vero, HeLa cells (both from ATCC, Manassas, VA) and Raw Lucia ISG (IFN-stimulated gene) cells (Invivogen, San Diego, CA) were cultured in DMEM with 10% FBS containing 2% penicillin-streptomycin (pen/strep). Cultures were maintained at 37°C with 5% CO_2 in a humidified incubator and tested periodically for mycoplasma contamination.

Microscopic detection of cGAS activation

HeLa cells were infected with Brazil A4 strain expressing H3-mNeon Green at a parasite/cell ratio of 10:1 for 3 h and fixed at various time points postinfection. Cells were stained with the mouse cGAS polyclonal Ab (Proteintech, Rosemont, IL) followed by a goat anti-mouse IgG (H+L) Alexa Fluor 594 (ThermoFisher Scientific, Waltham, MA) followed by DAPI to stain nuclear and kDNA. Cells mounted with ProLong Diamond anti-fade mounting solution (ThermoFisher Scientific) were imaged using the laser-scanning confocal microscope LSM 710 attached to an EXFO Xcite series 120Q lamp and a digital Zeiss XM10 camera.

Primary murine macrophage culture and quantification of IFN-β mRNA levels

Mouse bone marrow–derived macrophages (BMDMs) were generated by flushing the hind limb tibias and femurs of 8- to 12-wk-old mice with cold DMEM, and the recovered bone marrow progenitor cells were cultured in DMEM supplemented with 10% FBS in the presence of recombinant murine M-CSF (10 ng/ml; PeproTech, Cranbury, NJ) for 6 d, with frequent replacement of media containing cytokine every few days. BMDMs were infected with Brazil strain parasites at a parasite/cell ratio of 10:1 for 3 h, and total RNA was harvested 24 hpi using the Tri Reagent (Sigma-Aldrich, St. Louis, MO) and RNA clean and concentrator 5 (Zymo Research, Irvine, CA). cDNA was synthesized using the SuperScript III first-strand synthesis system (Invitrogen, Carlsbad, CA) using an Oligo (dT)20 primer. cDNA templates were used for a quantitative real-time PCR using iQ5 Multi-Color real-time PCR detection system with iQ5 Standard Edition Optical System Software version 2 (both from Bio-Rad, Hercules, CA). Primers used for IFN-β were 5′-GACCAACAAGTGTCTCCTCCAAA-3′ (forward) and 5′-AGCAAGTTGTAGCTCATGGAAAGAG-3′ (reverse).

Mouse fibroblast culture and IFN-β ELISA assay

Mouse fibroblasts were isolated and cultured from ear tissue clips. In brief, 1- to 2-mm pieces of ear clips from mice were sequentially rinsed well with Betadine (antimicrobial), 70% ethanol, and PBS (with pen/strep). Under sterile conditions in a six-well plate, each tissue was minced finely with a scalpel in 0.25 ml of Liberase TM (5 mg/ml in HBSS with Ca and Mg; Roche, Indianapolis, IN). An additional 0.25 ml collagenase mixture was added to the well and incubated for 30 min at 37°C, 5% CO_2. Six milliliters of DMEM (10% FBS + pen/strep) was added and incubated continually at 37°C, 5% CO_2 for 7–10 d with frequent replacement of media until cells have proliferated and were confluent. Mouse fibroblasts were infected with Brazil strain parasites at a parasite/cell ratio of 10:1 for 3 h, and the supernatants were collected at the indicated time points postinfection to assay the level of secreted IFN-β protein using the mouse IFN-β DuoSet ELISA kit (R&D Systems, Minneapolis, MN) according to the manufacturer's protocol.

IFN-β–GFP telomerase-immortalized human fibroblasts reporter cell assay

IFN-β–GFP telomerase-immortalized human fibroblasts (THF) reporter cells, a gift from Dr. K. L. Mossman (McMaster University, Hamilton, ON, Canada), were either infected or not with tdTomato-expressing CL strain parasites at a ratio of 5:1, or transfected with polyinosinic-polycytidylic acid [poly(I:C)] (Invivogen)/Lipofectamine 3000 (ThermoFisher Scientific) for 24 h under IFNAR blocking conditions using the anti-mouse IFNAR1 Ab (MAR1-5A3; BioXCell, Lebanon, NH). Cells were detached, and reporter activation was assessed using flow cytometry.

Detection of luciferase activity from cell-culture medium

Raw Lucia ISG cells (Invivogen) were used to assess the ability of *T. cruzi* to induce IRF activation under conditions of IFNAR blocking using the anti-mouse IFNAR1 Ab (MAR1-5A3; BioXCell). Reporter cells were either infected or not with Brazil strain parasites at a ratio of 5:1 for 16 h under IFNAR blocking conditions. Parasites and media were replaced and transfected with either DNA (IFN Stimulatory DNA; ISD naked) or 2,3-cGAMP (both Invivogen) using Lipofectamine 3000 (ThermoFisher Scientific) also under conditions of IFNAR blocking. Reporter activity was assayed 24 h poststimulation by the detection of secreted Lucia luciferase in 10 μl of culture medium after the addition of 50 μl QuantiLuc substrate (Invivogen) and immediate manual measurement of luciferase signal according to manufacturer's protocol using the Synergy H4 Hybrid plate reader (BioTek, Winooski, VT).

In vitro amastigote counting

Isolated BMDMs were infected with CL-tdTomato parasites at a parasite/cell ratio of 5:1 or 10:1 for 3 h. Cells were washed and fixed at defined days postinfection followed by DAPI staining. Images obtained using the Cytation

5 or Lionheart imager (both BioTek) and amastigotes counts were obtained using the Gen5 software.

In vivo imaging and quantification of parasite growth in the footpad

Mice were injected in the footpads with 250,000 tdTomato-expressing CL parasites per foot and anesthetized using 2.5% (v/v) gaseous isofluorane in oxygen before imaging on a Maestro imager (CRi, Beverly, MA). Quantification of fluorescence intensity and data analysis was performed using the Maestro Software.

Mouse injections

Injection with mouse IFN-β carrier-free (PBL Assay Science) s.c. in the infected footpads was at a dose of 2500 U per 10 μl. Anti-CCR2 mAb MC-21, a gift from Dr. M. Mack (University Hospital Regensburg, Regensburg, Germany), was administered by i.p. injection of 20 μg per mouse daily from 2 to 6 d postinfection (dpi). Neutrophil depletion was carried out by the injection of Anti-Ly6G (1A8; BioXCell) at a dose of 500 μg/mouse i.p. at 2 and 4 dpi. Recombinant Mouse CXCL1 (KC) (carrier-free; BioLegend, San Diego, CA) was injected s.c. to each infected footpad at 500 ng in 10 μl at 4 dpi.

Cell isolation and phenotyping

Mice were euthanized, and infected ears or hind footpad were collected at 6 dpi. Separated dorsal and ventral sheets of ears were incubated at 37°C for 90 min in 2 ml of Hanks' media with Ca^{2+} and Mg^{2+} containing 0.8 U/ml Liberase TL (Roche) and 160 U/ml DNase I (DNase I from bovine pancreas; Sigma). Ear tissue was dissociated by rubbing between two frosted glass slides and filtered using 40-μm filters (Falcon), pelleted via centrifugation, and stained for flow cytometry analysis. Cells were first stained for viability with Live/Dead Fixable Aqua Dead Cell Stain Kit (Invitrogen). The following anti-mouse Abs were used for staining: CD45.2-FITC (1:100; BioLegend), CD11b-allophycocyanin-eF780 (1:100; eBioscience/Invitrogen), and Gr1-PerCP Cyanine 5.5 (1;100; BioLegend). Samples were acquired using a CyAn flow cytometer (Beckman Coulter) or Cytoflex (Beckman Coulter) and analyzed with FlowJo (Tree Star) or FCS express software (De Novo).

Monitoring immune responses in peripheral blood

For assessing immune responses in the circulation of infected mice, blood was collected from the tail tips of mice into Alsever's solution and washed with PBS with 1% BSA and 0.05% sodium azide (PAB) (both from Sigma). Erythrocytes were selectively lysed medium of hypotonic ammonium chloride to lyse RBCs. Abs used were anti-CD8 FITC (1:800), anti-CD4-PECy5 (1:400), and CD44-eF450 (1:400) (all from BioLegend). TSKB20/Kb tetramers labeled with allophycocyanin were synthesized at the Tetramer Core Facility (Emory University, Atlanta, GA). Cells were stained at 4°C for at least 30 min and washed with PAB. Cells were acquired using a CyAn flow cytometer (Beckman Coulter) and analyzed with FlowJo software (Tree Star).

Quantification of parasite burden

Parasite equivalents in tissue were determined as previously described. In brief, mouse hind leg muscle tissue was collected and finely minced. Samples were incubated at 55°C in SDS–proteinase K lysis buffer. DNA was extracted twice with phenol:chloroform: isoamyl alcohol (25:24:1), precipitated with 100% ethanol, and resuspended in nuclease-free water. PCRs contained iQ SYBR Green Supermix (Bio-Rad) and primers specific for *T. cruzi* or mouse genomic DNA. Samples were analyzed on an iCycler (Bio-Rad), and *T. cruzi* equivalents were calculated as the ratio of *T. cruzi* satellite DNA divided by the quantity of mouse TNF-α DNA in each sample.

Imaging and quantification of parasite growth in the muscle

Mice were infected with 250,000 CL3-Luciferase parasites in the calf muscle. For bioluminescent detection, mice were injected via an i.p. route with D-luciferin (150 mg/kg; PerkinElmer, Waltham, MA) and anesthetized using 2.5% (v/v) gaseous isofluorane in oxygen before imaging on an IVIS 100 imager (Xenogen, Hopkinton, MA). Quantification of bioluminescence and data analysis were performed using Living Image v4.3 software (Xenogen). Infected hearts were clarified, processed, imaged, and quantified using light sheet microscopy as previously described (42).

Statistical analysis

Statistical significance was calculated between two groups by two-tailed Student *t* test, or between three or more groups by two-way ANOVA with Bonferroni multiple-comparison test using Prism 9.0.0 software (GraphPad Prism, San Diego, CA). Asterisks indicate values (mean ± SEM) that are significantly different between specified groups (*$p < 0.05$, **$p < 0.01$, ***$p < 0.001$, and ****$p < 0.0001$).

Results

T.cruzi *infection activates the cGAS–STING pathway in murine macrophages and fibroblasts to induce an IFN-I response*

To determine whether activation of the cGAS–STING pathway was instrumental in the IFN-I induction during *T. cruzi* infection, we first assessed cGAS activation in HeLa cells, which are reported to have a substantial basal expression of this sensor (43). Molecules of cGAS are primarily diffused in the cytosol at steady state but, once stimulated, aggregate to form puncta surrounding the DNA stimulus (44). Activated cGAS then uses cellular ATP and GTP as substrates to form the second messenger cGAMP, which binds to and activates STING. However, infection of HeLa cells with *T. cruzi* trypomastigotes failed to induce visible cGAS puncta formation, relative to cells transfected with DNA (Fig. 1A). Although small punctate forms are occasionally visible in infected cells, these were not at a significantly increased incidence to that observed in uninfected cells (Supplemental Fig. 1A).

The failure to detect cGAS puncta by microscopy could be related to the rather modest activation of this pathway by *T. cruzi* infection. To further explore whether the cGAS–STING pathway was involved in IFN-I production after *T. cruzi* infection, we compared the IFN-β transcript levels in *T. cruzi*–infected primary BMDMs from STING-deficient ($STING^{Gt}$-Goldenticket), $cGAS^{-/-}$, and wild-type (WT) C57BL/6 (B6) mice at 24 hpi. Our laboratory and others have observed that the primary host cell type infected by *T. cruzi* at the initial site of infection in the skin is a resident macrophage, which is also permissive to parasite growth (15, 45). *T. cruzi* infection induced substantial amounts of IFN-β mRNA in WT macrophages, but macrophages from $STING^{Gt}$ or $cGAS^{-/-}$ mice had ~4- to >10-fold lower levels (Fig. 1B). Furthermore, in infections of nonimmune cells (primary murine fibroblasts), the absence of either cGAS or STING completely abolished IFN-β secretion measured at both 24 and 72 hpi (Fig. 1C). Together, these results demonstrate that cGAS activation is largely responsible for the STING-dependent induction of IFN-I during *T. cruzi* invasion.

Modest IFN-β induction during infection is likely a consequence of limited stimulation, rather than active suppression of the STING pathway

We next questioned whether the overall limited level of *T. cruzi*–elicited IFN-I results from the modest triggering of the pathway in most infected cells or the relatively strong induction in only a small subset of infected cells; the latter demonstrated to be the case in certain viral infections (46–48). To quantify the frequency and level of IFN-I–producing cells during *T. cruzi* infection, we used a THF cell line with a stably integrated GFP reporter controlled by the IFN-β promoter sequence (IFN-β–GFP THFs) (46). To directly assess infection-driven IFN-I production without the interference from IFN-I signaling, we assayed reporter activity under IFN-α/β receptor subunit 1 (IFNAR1) blocking conditions using the MAR1-5A3 mAb. When IFN-β–GFP THFs were infected with tdTomato-expressing parasites under IFNAR blocking conditions, only a slight shift in the GFP expression was consistently detected in infected cells at 16 hpi relative to the uninfected cells in the same sample. The modest IFN-β levels observed during infection contrasts with the vigorous induction levels observed in cells stimulated with the RIG agonist poly(I:C) (Fig. 2A). Thus, *T. cruzi* invasion of host cells consistently triggers a low-level IFN-I response.

The generally subdued host response to cell invasion by *T. cruzi* has been attributed to parasite modulation of infected host cells (49–51). To indirectly assess the potential for parasite interference of cGAS–STING pathway activation, we investigated the ability of *T. cruzi*–infected macrophages to respond to exogenous stimulation by pathway agonists, relative to uninfected cells. For this, we used

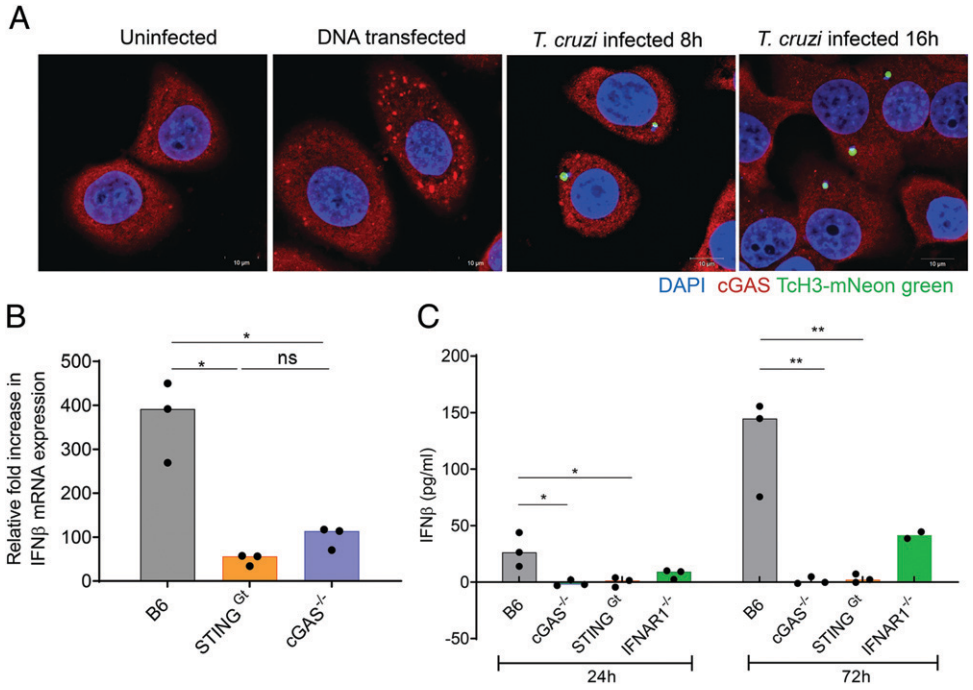

FIGURE 1. *T. cruzi* activates the cGAS–STING pathway in primary cells to induce a modest IFN-I response. (**A**) Microscopic detection of cGAS activation in uninfected, DNA-transfected, and infected HeLa cells 8 h posttransfection and 8 and 16 hpi. Cells were transfected with DNA (2 μg/ml). Cells were infected with transgenic *T. cruzi* overexpressing a histone 3 (TcCLB.509471.59)-mNeon green fusion protein, which localizes in the parasite nucleus. (**B**) The IFN-β transcript levels of BMDMs from B6, STING^{Gt}, and cGAS$^{-/-}$ mice infected with *T. cruzi* and measured by quantitative RT-PCR at 24 hpi. Values reported are normalized to GAPDH transcript levels and expressed as a fold change compared with uninfected controls. Data are representative of two independent experiments of $n = 3$ infection replicates. (**C**) The levels of IFN-β in supernatants from infected primary mouse fibroblasts were quantified using ELISA after 24 and 72 h. Data are representative of two independent experiments of $n = 2$–3 infection replicates. *$p < 0.05$, **$p < 0.01$.

IRF reporter macrophages that respond to both IFN-I induction and IFN-I signaling by the secretion of luciferase. To assess solely modulation at the level of IFN-I induction rather than IFN-I signaling, we again assayed reporter activity in the presence of MAR1-5A3 blocking Ab. The extent of IFNAR blocking of these reporter cells was assessed by the addition of increasing amounts of recombinant murine IFN-β; >10 U/ml of the cytokine was effectively inhibited (Supplemental Fig. 1B). Under conditions of IFNAR1 blocking,

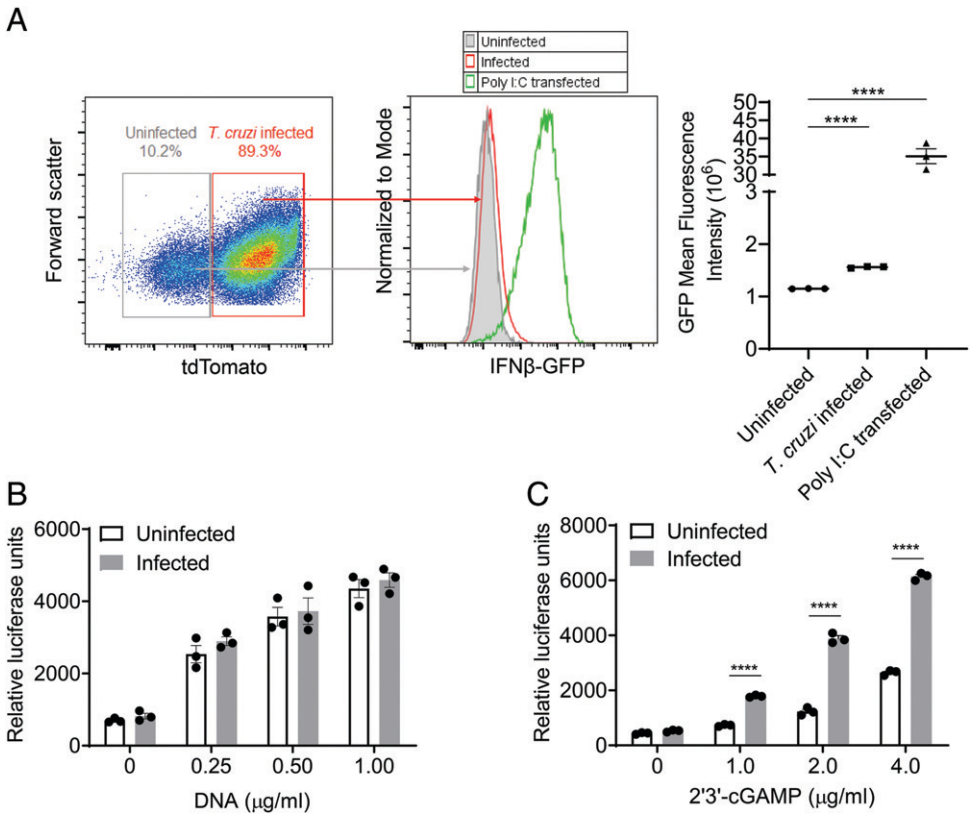

FIGURE 2. Modest IFN-β levels are induced in all infected cells and are not a consequence of active parasite suppression of the pathway. (**A**) IFN-β–GFP reporter THF cells were infected with tdTomato-expressing CL *T. cruzi* or transfected with poly(I:C) for 16 h under IFNAR blocking conditions. The level of reporter expression in tdTomato −ve (uninfected) or tdTomato +ve (infected) cell subsets within a representative infected sample is displayed alongside levels of reporter activation after poly(I:C) transfection as measured by flow cytometry. The mean florescence intensities are displayed (right). (**B** and **C**) IRF reporter macrophage activation by transfected DNA (B) or IFN-β (C) in previously infected (for 16 h) or uninfected cells to stimulation. All data are representative of two or more independent experiments of $n = 3$ infection replicates. ****$p < 0.0001$.

cells either infected for 16 h or uninfected responded equivalently to transfection with various amounts of DNA (Fig. 2B). Moreover, after direct STING activation with a nucleotide agonist 2′3′-cGAMP, *T. cruzi*–infected cells responded to a higher level than uninfected cells, demonstrating synergistic enhancement of IFN-I induction upon STING activation after *T. cruzi* infection (Fig. 2C). Similar results were observed when cells were infected and stimulated simultaneously with either DNA or 2′3′-cGAMP (Supplemental Fig. 1C, 1D). Because infection did not appear to limit cGAS–STING pathway activation to exogenous stimulation, these data provide no evidence of suppression of this pathway after cell invasion by *T. cruzi*. Together with the limited microscopic detection of cGAS activation postinfection (Fig. 1A), and the ability to detect IFN-β transcript and protein levels postinfections with relatively high parasite/host cell ratios (Fig. 1B, 1C), our data indicate that the modest IFN-β induction is likely a consequence of limited induction of the cGAS–STING pathway by *T. cruzi* infection of host cells.

Activation of the cGAS–STING pathway initially restricts amastigote growth but ultimately promotes parasite expansion at the site of infection

The best-characterized impact of cGAS and STING activation is the immune defense functions of ISGs induced downstream of this pathway (29, 52). Therefore, we investigated the involvement of cGAS–STING and IFN-I signaling on parasite growth in vitro in primary macrophage cultures. As expected, in the deficiency of cGAS, STING, or IFNAR1, intracellular amastigote growth was significantly greater as compared with that in WT B6 macrophages (Fig. 3A). In addition, supplementing IFN-β to infected cGAS$^{-/-}$ or STING^{Gt} macrophages reduced amastigote numbers to the levels observed in WT B6 macrophages (Fig. 3B). These results confirm that both cGAS and STING act to constrain amastigote numbers in host cells through an IFN-I–dependent mechanism.

A growth restrictive impact of the cGAS–STING–IFN-I was also evident in vivo, at least very early in infection (Fig. 3C). Parasite growth at the site of inoculation in footpads was inferred by

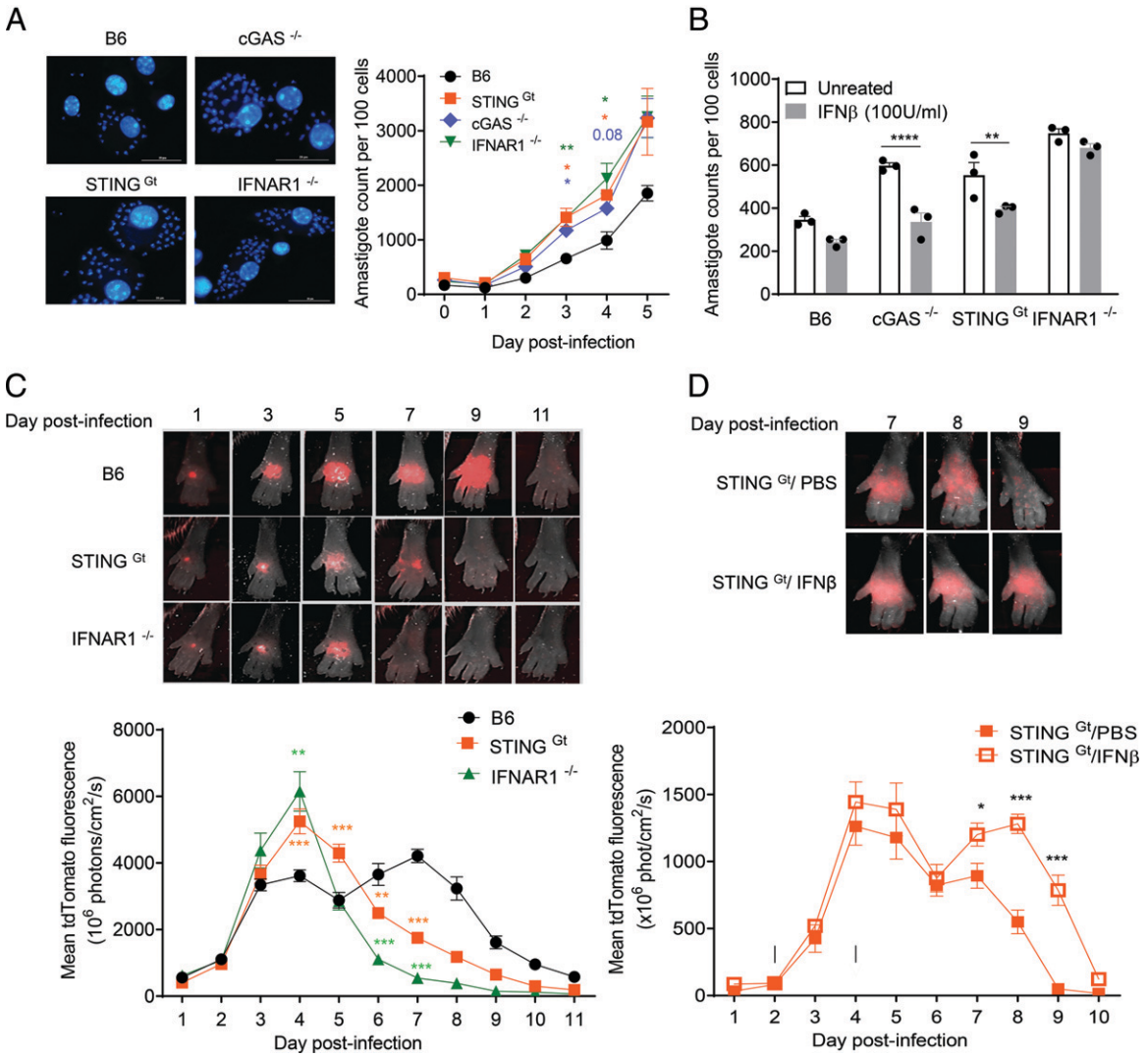

FIGURE 3. Activation of the cGAS–STING pathway restricts intracellular parasite growth in vitro but promotes parasite expansion at the infection site. (**A**) In vitro parasite growth in primary BMDMs from B6, cGAS$^{-/-}$, STING^{Gt}, and IFNAR1$^{-/-}$ mice with representative images at 3 dpi (left) and amastigote counts (right). $n = 3$ replicate infections. (**B**) Amastigote counts at 3 dpi with or without treatment of infected BMDMs with IFN-β (100 U/ml) added after 3 h of infection with parasites. $n = 3$ replicate infections. (**C**) Differential parasite growth kinetics of STING^{Gt} and IFNAR1$^{-/-}$ compared with B6 mice infected with tdTomato-expressing parasites in each footpad and quantification of fluorescence intensity to assess parasite levels daily postinfection. Infected footpads were imaged, and fluorescence intensity was quantified. Representative images of infected feet at different time points postinfection (top) and quantification of mean fluorescence intensity (bottom). $n = 5$–6 mice (10–12 footpads). (**D**) Parasite growth kinetics of STING^{Gt} mice after footpad injections with PBS or recombinant mouse IFN-β at 2 and 4 dpi (represented by black vertical bars). Values reported are from $n = 5$ mice (10 footpads). All data are representative of two or more independent experiments. *$p < 0.05$, **$p < 0.01$, ***$p < 0.001$, ****$p < 0.0001$.

quantifying the change in fluorescence intensity of tdTomato-expressing parasites. *T. cruzi* growth at the infection site is initially relatively synchronous, displaying two peaks of intensity over 8–10 d in WT mice. The two peaks correspond to intracellular amastigote proliferation for 4–5 d, followed by trypomastigote release, reinfection, and replication within a new set of host cells (15). As expected, in the absence of STING and IFN-I signaling, parasite growth was significantly greater during the first round of host cell infection, peaking at day 4. Counterintuitively, in both $STING^{Gt}$ and $IFNAR1^{-/-}$ mice, a second round of infection and expansion was reduced or entirely unapparent. A detectable second round of invasion and replication could be established in $STING^{Gt}$ mice by administration of rIFN-β at the infection site (Fig. 3D). These results demonstrate that the *T. cruzi*–induced, STING-dependent production of IFN-I initially restricts but ultimately promotes parasite expansion at the initial site of infection.

IFN-I–mediated parasite expansion at the inoculation site is correlated with increased monocyte and decreased neutrophil infiltration

We next investigated the mechanism of the IFN-I–mediated parasite growth enhancement or the otherwise improved parasite control in the absence of this response. Previous studies demonstrate that the induction and recruitment of parasite-specific $CD4^+$ and $CD8^+$ T cell responses rigorously control parasite numbers in B6 mice at the initial site by 10–12 dpi (15). However, the generation of *T. cruzi*–specific $CD8^+$ and activated $CD4^+$ T cells was not accelerated in $STING^{Gt}$ or $IFNAR1^{-/-}$ mice (Supplemental Fig. 2A, 2B) (53), suggesting that STING impacts parasite growth before the development of these adaptive immune effectors. Resident macrophages are infected and permissive to *T. cruzi* amastigote growth at the site of infection (15), and one downstream effect of IFN-I is the recruitment of monocytes through the induction of monocyte chemoattractants such as CCL2 and CCL7 (54), both of which are also upregulated at the *T. cruzi* infection site (17). We thus hypothesized that IFN-I acts to recruit infection-permissive monocytes to the initial site of infection, and in the absence of that STING-driven IFN-I production, the second round of parasite expansion at the site is reduced.

To address this hypothesis, we first phenotyped immune cells recruited to the site of infection in the ear pinnae in the presence and absence of STING and IFN-I signaling using markers previously used for identification of distinct immune subsets (Supplemental Fig. 3) (15). We consistently observed a decreased proportion of inflammatory monocytes ($CD45^+CD11b^{Hi}Gr1^{Int}$) recruited to the site in $STING^{Gt}$, and even more so in the absence of IFN-I signaling, at day 6 postinfection (Fig. 4A). This reduction is also evident in the infected cell populations, because there were also significantly fewer *T. cruzi* $tdTomato^+$–infected monocytes at the infection site in $STING^{Gt}$ and $IFNAR1^{-/-}$ mice (Fig. 4B). Also notable is the increased proportion of recruited and infected neutrophils at the site in $IFNAR1^{-/-}$ (Fig. 4A, 4B). Similar results were observed with absolute counts of total and infected subpopulations as well. These results suggest a positive correlation of parasite growth with monocyte recruitment in both $STING^{Gt}$ and $IFNAR1^{-/-}$ strains and in the absence of monocytes, the influx and infection of neutrophils in $IFNAR1^{-/-}$ mice.

Depletion of differentially infiltrating cells had a minimal impact on parasite growth at the infection site

We next specifically depleted inflammatory monocytes in B6 mice to determine whether the loss of recruited monocytes in $STING^{Gt}$ and $IFNAR1^{-/-}$ was the limiting factor for parasite expansion. Administration of an anti-CCR2 mAb MC-21 (55) to B6 mice decreased the proportion of inflammatory monocytes recruited to the site by >50% at day 6 postinfection (Fig. 5A), yet surprisingly, this depletion did not significantly alter parasite growth (Fig. 5B). Conversely, we asked whether the observed increase in neutrophil influx in $STING^{Gt}$ and $IFNAR1^{-/-}$ mice is responsible for improved parasite control in these mice, because neutrophils are known to be key players in indirectly enhancing effector function of infected cells such as macrophages or directly killing extracellular parasites via a mechanism like neutrophil extracellular trap formation (56). Depletion of neutrophils in $STING^{Gt}$ using the anti-mouse Ly6G mAb 1A8 resulted in >70% reduction of circulating neutrophils (Fig. 5C) yet no detectable enhancement in parasite growth at the site (Fig. 5D). Collectively, the lack of impact on parasite growth by Ab-mediated depletion of inflammatory monocytes and/or neutrophils indicates that either a more complete depletion of cell types must be achieved to observe an impact on parasite growth, or that there is a more complex interplay of multiple cellular effectors controlling parasite expansion at the infection site.

STING activation does not impact the initial establishment of infection or long-term parasite persistence but constrains acute parasite load in the heart independently of IFN-I

We next explored the possible consequences of STING-driven enhancement of *T. cruzi* expansion at the infection site and first considered whether the reduction in parasite numbers at the initial site of infection observed in the absence of IFN-I signaling might compromise the establishment of a persistent, systemic infection. To test this hypothesis, we infected mice with a low number of parasites (five per animal), a dose we had previously determined would result in a systemic infection in the majority of, but not all, WT mice (Supplemental Fig. 4A). However, the deficiency or absence of STING and IFN-I signaling had no detectable impact on the successful establishment of systemic infection as determined by detection of parasites in the skeletal muscle after this low-dose infection (Supplemental Fig. 4B). Second, if STING pathway activation enhances parasite numbers not only at the initial infection site but also at subsequent (systemic) sites of parasite development, then an overall decrease in tissue parasite load systemically might be expected in $STING^{Gt}$ mice. However, chronically infected $STING^{Gt}$ mice displayed no significant difference in parasite loads in skeletal muscle relative to WT mice (Fig. 6A). Thus, although STING disruption alters the early kinetics of *T. cruzi* development at the initial infection site, the deficiency or absence of STING or IFNAR1 does not appear to impact the overall establishment or skeletal muscle tissue-level persistence of *T. cruzi* in these infection models.

However, in the heart, where parasite persistence is correlated with the manifestation of clinical disease (57–59), a STING-dependent impact on parasite numbers was observed during acute infection. When parasite loads peak in the heart, previously determined to be ~15 dpi in WT mice (42), infected $STING^{Gt}$ and $cGAS^{-/-}$ hearts harbored significantly increased numbers of parasites and parasite-infected cells compared with B6 counterparts, as detected by tissue PCR and visualized by light-sheet fluorescent microscopy of whole clarified hearts (Fig. 6B, 6C, Supplemental Fig. 4C). Surprisingly, increased parasite levels were not observed in $IFNAR1^{-/-}$ mice, which displayed comparable or decreased heart parasite loads to B6 mice. In addition, the comparatively increased parasite numbers in $STING^{Gt}$ mice were not observed in the hearts at day 7 or 35 postinfection, demonstrating that STING activation has a significant, yet transient impact on the control of peak parasite burden in the heart (Supplemental Fig. 4D). Furthermore, because parasites are frequently found to persist in skeletal muscle tissue, we tracked the kinetics of parasite growth after direct infection of the mouse calf muscle (gastrocnemius) with luciferase-expressing parasites (Fig. 6D). A significant IFN-I–dependent initial growth restriction

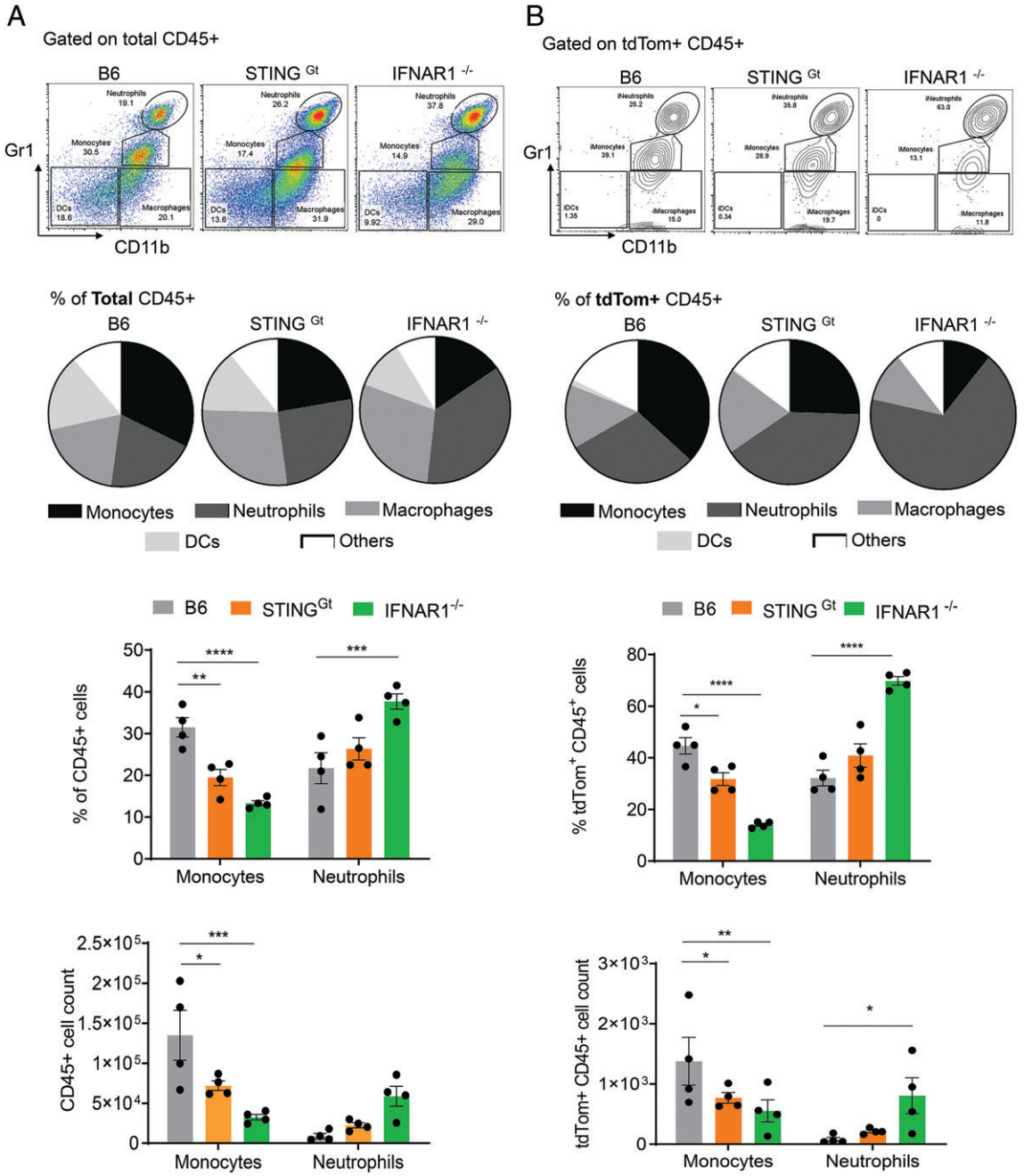

FIGURE 4. STING activation at the infection site results in a differential infiltration of monocyte and neutrophils. Cells recruited to the ears of mice infected at the site with tdTomato-expressing parasites were isolated at 5 dpi and immunophenotyped using the gating strategy described in Supplemental Fig. 3A. Differences in the proportion of (**A**) total or (**B**) infected (tdTom$^+$) CD45$^+$ leukocyte subsets in B6, STING^{Gt}, and IFNAR1$^{-/-}$ are shown. Representative flow plots (top) denote populations of monocytes (CD45$^+$CD11b^{Hi}Gr-1^{Int}), neutrophils (CD45$^+$CD11b^{Hi}Gr-1^{Hi}), macrophages (CD45$^+$CD11b^{Hi}Gr-1^{lo}), and DCs (CD45$^+$CD11b^{lo}Gr-1^{lo}). Pie charts (middle) show average (of $n = 4$ mice) proportions of each population in the different mouse groups, and bar graphs (bottom) show significant differences in the proportion and absolute count of monocyte and neutrophil subsets. Data are representative of two or more independent experiments. *$p < 0.05$, **$p < 0.01$, ***$p < 0.001$, ****$p < 0.0001$.

followed by parasite growth enhancement was seen in the skeletal muscle, with similar kinetics to that observed previously in the footpads. However, a STING deficiency had no significant impact on parasite levels in the skeletal muscle compared with B6 counterparts. This result is consistent with the fact that skeletal muscle tissue has a nearly undetected basal expression of STING (Supplemental Fig. 4E) (60). Together, these data indicate that the *T. cruzi*–elicited cGAS–STING pathway activation serves to restrict parasite levels in the heart before the generation and recruitment of parasite-specific T cell effectors. However, STING expression had no detectable impact on parasite control in the skeletal muscle, a major site of parasite persistence during chronic infection.

Discussion

The initial response of host cells to invasion by *T. cruzi* consists primarily of a IFN-I–driven gene expression program, with IRGs representing >30% of the total induced host genes (16, 17). During the preparation of this manuscript, de Souza Vieira et al. (24) reported

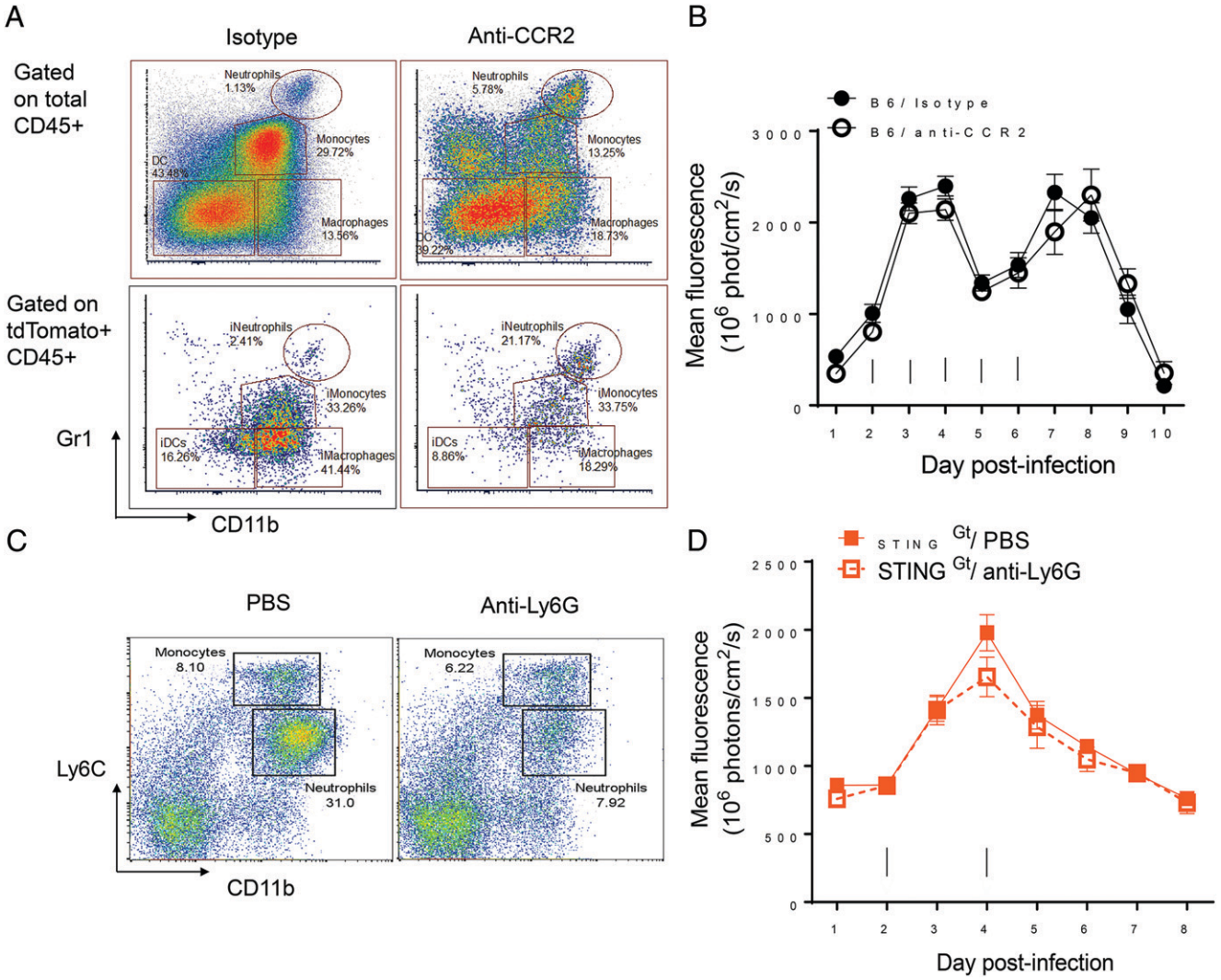

FIGURE 5. Specific depletion or augmentation of cellular recruitment had limited impact on parasite growth at the infection site. (**A**) Specific depletion of monocytes in B6 mice by i.p. injection with either isotype control or anti-CCR2 (MC-21) Ab as demonstrated by representative flow plots of the cellular infiltrate at the infection site at 6 dpi. (**B**) Parasite growth kinetics at the site of infection in WT mice with and without monocyte depletion, with black arrowheads representing the timing of treatment. $n = 4–5$ mice/group. (**C**) Specific depletion neutrophils in STING^{GT} mice by i.p. administration of either PBS or anti-Ly6G (mAb 1A8) at 2 and 4 dpi, demonstrated by peripheral blood staining at 5 dpi. (**D**) Parasite growth kinetics after neutrophil depletion postinfection, with black vertical bars representing the timing of treatment. $n = 4–5$ mice. Data are representative of two independent experiments.

that *T. cruzi*–elicited IFN-I induction is STING dependent. In this article, we confirm this observation and further elucidate the mechanism of IFN-I induction, demonstrating the involvement of the DNA sensor cGAS in the activation of the STING pathway during *T. cruzi* invasion.

The *T. cruzi*–elicited IFN-I response is relatively modest, as indicated by the absence of microscopic visualization of cGAS puncta, but it appears to be uniformly triggered, because an IFN-β reporter line showed low-level GFP expression in nearly all infected cells. Both of these patterns are in contrast with the heterogenous yet robust induction of IFN-β in a small subset of cells, as is the case for some viral infections (47, 48). This modest response evident at the individual cell level with *T. cruzi* infection is also observed at the population level; the 2- to 20- fold ISG induction in *T. cruzi*–infected cells (16) contrasts with the 4- to 150-fold increase in ISGs induced in the same cell type by the DNA virus CMV (14).

Most importantly, the relative weakness of this IFN-I–driven response in *T. cruzi*–infected cells is a result of a limited triggering of the STING pathway, rather than an active suppression of the pathway. This "failure to activate" model is in contrast with the "trigger-and-suppress" mechanism of evading host cell responses sometimes attributed to *T. cruzi* (49–51, 61) and employed by other intracellular parasites. The best characterized of these, *Toxoplasma gondii*, uses a cadre of secreted effectors to inhibit various host response molecules (reviewed in Ref. 62). These observations add additional support to the evidence that *T. cruzi* infection of host cells is a relatively quiet process that avoids a rapid and robust innate immune response (15, 63, 64). However, the question of whether *T. cruzi* lacks the potential to strongly activate host PRR, as we favor, or actively evades intracellular detection is likely to remain active until more is understood about amastigote biology and/or genome-wide screens for potential suppressors of parasite detection are possible.

Although modest, the IFN-I response upon *T. cruzi* infection is not inconsequential. However, the impact is quite complex. STING activation constrains intracellular *T. cruzi* replication in vitro, and during the initial round of replication, predominantly in resident macrophages (15), in vivo. However, STING activation-driven IFN-I at the initial infection site also modulates the site's cellular composition so as to enhance the overall parasite production therein through the recruitment of additional monocyte/macrophages. In the

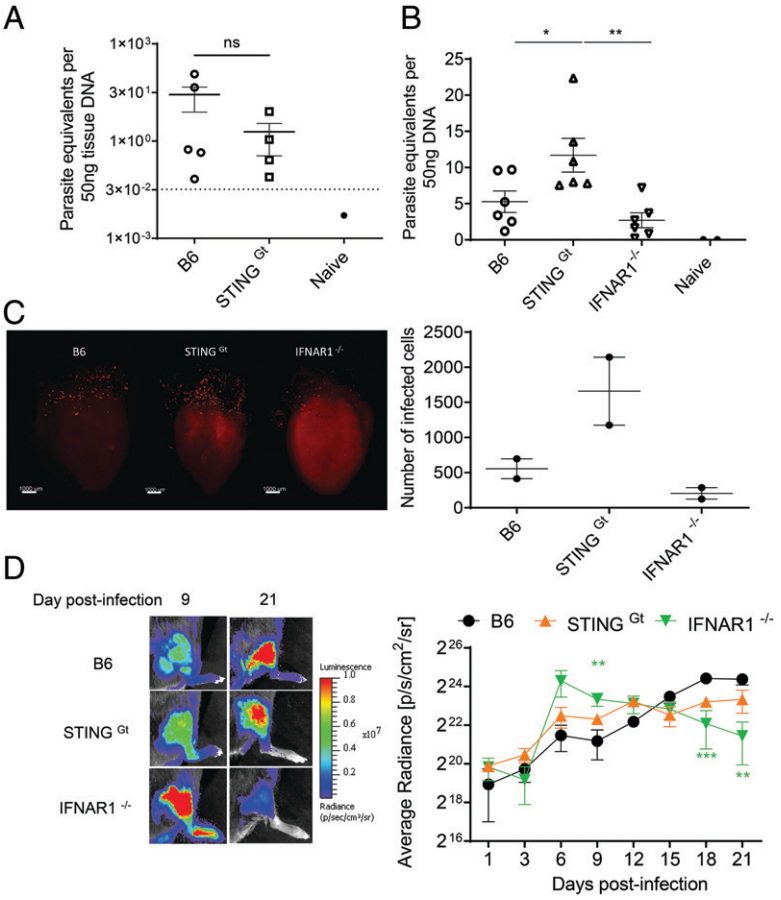

FIGURE 6. STING activation does not impact the initial establishment of infection or long-term parasite persistence but constrains acute parasite load in the heart independently of IFN-I. (**A**) The overall control of infection as determined by quantification of parasite loads in the skeletal muscle >300 d after footpad infection in B6 and STING^{Gt} mice. $n > 4$ mice per group. The dotted line represents the threshold of detection for the assay. (**B**) *T. cruzi* DNA in the hearts of B6, STING^{Gt}, and IFNAR1$^{-/-}$ mice infected i.p. with 200,000 Colombiana strain parasites as determined by quantitative real-time PCR at 14 dpi. $n = 6$ mice per group. (**C**) Light-sheet microscopic detection of tdTomato-expressing parasites in clarified hearts of B6, STING^{Gt}, and IFNAR1$^{-/-}$ mice 14 dpi with 200,000 Colombiana strain parasites. Representative images (left) with quantification (right) of $n = 2$ mice per group. (**D**) Parasite growth kinetics in the calf muscle of B6, STING^{Gt}, and IFNAR1$^{-/-}$ after direct infection of the gastrocnemius with parasites expressing luciferase determined by bioluminescence intensity. Representative images (left) and luminescent intensity with time (right). $n > 4$ mice per infection. All data are representative of two independent experiments. $*p < 0.05$, $**p < 0.01$, $***p < 0.001$.

absence of STING activation, more neutrophils and fewer monocytes are recruited, and parasite numbers at the site decline.

Trypomastigotes produced by these early rounds of cell infection and parasite replication at the initial infection site seed other tissues, generating a systemic infection. We hypothesized that the STING-influenced amplification of parasites at the inoculation site might increase the efficiency of establishment and propagation of infections in hosts. However, we were unable to demonstrate such a consequence using a low-infective dose regimen resembling natural infection; parasites successfully disseminated from the infection site, established systemically, and persisted long term equally well in STING^{Gt} and WT mice. Whether increased parasite numbers at the initial infection sites might favor parasite establishment postinfection by other relevant routes such as mucosal or oral routes, or perhaps impact acute-phase tissue damage and thereby the overall progression of disease throughout the infection, warrants further investigation.

Consistent with the findings of de Souza Vieira et al. (24), we found that STING activation restricted *T. cruzi* parasite levels in the heart, which is evident only at the peak of infection in that tissue. Because the presence and number of parasites in the acute phase has been associated with the severity of chronic phase disease in mice (57, 65–67), it is conceivable that even modestly increased parasite loads, and/or the associated inflammation, might impact disease manifestation in a vital organ such as the heart. Also, although not often symptomatic in humans, acute-phase infection can result in severe cardiac damage in both humans and other animals (68, 69). In such cases, STING activation might be expected to reduce infection, disease development, and perhaps even acute-phase death.

The stimulus for STING activation in *T. cruzi*–infected cells is not known. During host cell invasion, *T. cruzi* can undergo an asymmetric division that results in the deposition of the trypomastigote flagellum, and its associated DNA-containing kinetoplast, into the host cell cytoplasm, making this kDNA a strong candidate for the stimulus that drives the STING-dependent IFN-I response in *T. cruzi*–infected cells (25). However, the infrequent detection of cytoplasmic kDNA, as well as the limited ability to detect cGAS activation in infected cells via microscopy, has made a direct assessment of this possibility challenging. cGAS activation has also been reported to be induced by extracellular vesicles purified from the supernatants of *T. cruzi*–infected cultures and plasma of infected patients (70), although the relevance of such a mechanism in the induction of IFN-I during infection in vivo is unclear. The variable basal expression of STING in different tissues [high in heart, moderate in skin, and undetected in skeletal muscle and gut (71), the latter two major sites of *T. cruzi* persistence in chronic infections (72)], could impact tissue-specific parasite replication and persistence, similar to that of other PRRs involved in immune surveillance at barrier sites and in homeostasis and repair of infection-associated damage within vital organs such as the heart (73–75). These results highlight a previously undervalued tissue-specific impact of innate sensors in the detection of and response to pathogens that may potentially impact the overall outcome of infection, an important consideration for pathogens displaying distinct tissue tropisms or prevalence.

This study supports our growing understanding of the general stealth nature of the *T. cruzi* invasion that likely enables *T. cruzi* to persist successfully for the lifetime of its hosts (15, 63). The model that emerges from this and previous studies is that the relative quiet infection mode of *T. cruzi* results in a muted innate response, allowing systemic distribution of parasites from the initial infection site. But this limited response to cell invasion has impact beyond the initial infection site and likely applies to any "new" foci of infection that occur constantly throughout this persistent infection.

Altogether, our study demonstrates that detection of *T. cruzi* by the STING pathway has distinct consequences in restricting parasite

loads in different sites and tissues relevant to the infection process. Apart from a significant STING-mediated restriction of *T. cruzi* in the heart, the lack of an overall impact of *T. cruzi*–elicited STING activation is perhaps due to multiple factors, including its rather modest induction levels, the low basal expression of STING in most distal sites that parasites frequently replicate in, and the lack of an impact of the STING activation in affecting the generation of parasite-specific effectors that are the ultimate controllers of infection. A further understanding of the site-specific detection of *T. cruzi* infection could reveal potential factors that lead to the prolonged persistence and pathology of this infection and opportunities for therapeutic interventions.

Acknowledgments

We thank Dr. Angel Padilla for technical assistance with in vivo experiments, Dr. Wei Wang for producing the TcH3-mNeon *T. cruzi* line, as well as the other members of the Tarleton research group for overall support and helpful suggestions. We also thank Dr. Matthias Mack and Dr. Karen L. Mossman for the gifts of critical reagents and acknowledge Julie Nelson of the Center for Tropical and Emerging Global Diseases Cytometry Shared Resource Laboratory and Dr. Muthugapatti Kandasamy of the Center for Tropical and Emerging Global Diseases Biomedical Microscopy Core for expertise and assistance.

Disclosures

The authors have no financial conflicts of interest.

References

1. Jain, A., and C. Pasare. 2017. Innate control of adaptive immunity: beyond the three-signal paradigm. *J. Immunol.* 198: 3791–3800.
2. Sullivan, B. M., J. R. Teijaro, J. C. de la Torre, and M. B. Oldstone. 2015. Early virus-host interactions dictate the course of a persistent infection. *PLoS Pathog.* 11: e1004588.
3. Frolov, I., M. Akhrymuk, I. Akhrymuk, S. Atasheva, and E. I. Frolova. 2012. Early events in alphavirus replication determine the outcome of infection. *J. Virol.* 86: 5055–5066.
4. Subbian, S., N. Bandyopadhyay, L. Tsenova, P. O'Brien, V. Khetani, N. L. Kushner, B. Peixoto, P. Soteropoulos, J. S. Bader, P. C. Karakousis, et al. 2013. Early innate immunity determines outcome of *Mycobacterium tuberculosis* pulmonary infection in rabbits. *Cell Commun. Signal.* 11: 60.
5. Pontiroli, F., O. Dussurget, I. Zanoni, M. Urbano, O. Beretta, F. Granucci, P. Ricciardi-Castagnoli, P. Cossart, and M. Foti. 2012. The timing of IFNβ production affects early innate responses to *Listeria monocytogenes* and determines the overall outcome of lethal infection. *PLoS One* 7: e43455.
6. Cheemarla, N. R., T. A. Watkins, V. T. Mihaylova, B. Wang, D. Zhao, G. Wang, M. L. Landry, and E. F. Foxman. 2021. Dynamic innate immune response determines susceptibility to SARS-CoV-2 infection and early replication kinetics. *J. Exp. Med.* 218: e20210583.
7. Channappanavar, R., A. R. Fehr, J. Zheng, C. Wohlford-Lenane, J. E. Abrahante, M. Mack, R. Sompallae, P. B. McCray, Jr., D. K. Meyerholz, and S. Perlman. 2019. IFN-I response timing relative to virus replication determines MERS coronavirus infection outcomes. *J. Clin. Invest.* 129: 3625–3639.
8. Cadena, A. M., J. L. Flynn, and S. M. Fortune. 2016. The importance of first impressions: early events in *Mycobacterium tuberculosis* infection influence outcome. *MBio* 7: e00342-16.
9. Hilleman, M. R. 2004. Strategies and mechanisms for host and pathogen survival in acute and persistent viral infections. *Proc. Natl. Acad. Sci. USA* 101(Suppl. 2): 14560–14566.
10. Boldogh, I., T. Albrecht, and D. D. Porter. 1996. Persistent viral infections. In *Medical Microbiology*, 4th Ed. S. Baron, ed. University of Texas Medical Branch at Galveston, Galveston, TX.
11. Jenner, R. G., and R. A. Young. 2005. Insights into host responses against pathogens from transcriptional profiling. *Nat. Rev. Microbiol.* 3: 281–294.
12. Tarleton, R. L. 2015. CD8+ T cells in *Trypanosoma cruzi* infection. *Semin. Immunopathol.* 37: 233–238.
13. Padilla, A. M., J. M. Bustamante, and R. L. Tarleton. 2009. CD8+ T cells in *Trypanosoma cruzi* infection. *Curr. Opin. Immunol.* 21: 385–390.
14. Zhu, H., J. P. Cong, G. Mamtora, T. Gingeras, and T. Shenk. 1998. Cellular gene expression altered by human cytomegalovirus: global monitoring with oligonucleotide arrays. *Proc. Natl. Acad. Sci. USA* 95: 14470–14475.
15. Padilla, A. M., C. Rosenberg, P. Cook, F. Sanchez-Valdez, C. McElhannon, and R. L. Tarleton. 2023. Delayed activation of T cells at the site of infection facilitates the establishment of *Trypanosoma cruzi* in both naive and immune hosts. *MSphere* 8: e0060122.
16. Vaena de Avalos, S., I. J. Blader, M. Fisher, J. C. Boothroyd, and B. A. Burleigh. 2002. Immediate/early response to *Trypanosoma cruzi* infection involves minimal modulation of host cell transcription. *J. Biol. Chem.* 277: 639–644.
17. Chessler, A. D., M. Unnikrishnan, A. K. Bei, J. P. Daily, and B. A. Burleigh. 2009. *Trypanosoma cruzi* triggers an early type I IFN response in vivo at the site of intradermal infection. *J. Immunol.* 182: 2288–2296.
18. Campos, M. A., I. C. Almeida, O. Takeuchi, S. Akira, E. P. Valente, D. O. Procópio, L. R. Travassos, J. A. Smith, D. T. Golenbock, and R. T. Gazzinelli. 2001. Activation of Toll-like receptor-2 by glycosylphosphatidylinositol anchors from a protozoan parasite. *J. Immunol.* 167: 416–423.
19. Bafica, A., H. C. Santiago, R. Goldszmid, C. Ropert, R. T. Gazzinelli, and A. Sher. 2006. Cutting edge: TLR9 and TLR2 signaling together account for MyD88-dependent control of parasitemia in *Trypanosoma cruzi* infection. *J. Immunol.* 177: 3515–3519.
20. Oliveira, A. C., B. C. de Alencar, F. Tzelepis, W. Klezewsky, R. N. da Silva, F. S. Neves, G. S. Cavalcanti, S. Boscardin, M. P. Nunes, M. F. Santiago, et al. 2010. Impaired innate immunity in Tlr4($^{-/-}$) mice but preserved CD8+ T cell responses against *Trypanosoma cruzi* in Tlr4-, Tlr2-, Tlr9- or Myd88-deficient mice. *PLoS Pathog.* 6: e1000870.
21. Tarleton, R. L. 2007. Immune system recognition of *Trypanosoma cruzi*. *Curr. Opin. Immunol.* 19: 430–434.
22. Pulendran, B., and R. Ahmed. 2006. Translating innate immunity into immunological memory: implications for vaccine development. *Cell* 124: 849–863.
23. Chessler, A. D., L. R. Ferreira, T. H. Chang, K. A. Fitzgerald, and B. A. Burleigh. 2008. A novel IFN regulatory factor 3-dependent pathway activated by trypanosomes triggers IFN-beta in macrophages and fibroblasts. *J. Immunol.* 181: 7917–7924.
24. de Souza Vieira, R., M. S. Nascimento, I. H. Noronha, J. R. C. Vasconcelos, L. A. Benvenuti, G. N. Barber, N. O. S. Câmara, J. Kalil, E. Cunha-Neto, and R. R. Almeida. 2022. STING signaling drives production of innate cytokines, generation of CD8$^+$ T cells and enhanced protection against *Trypanosoma cruzi* infection. *Front. Immunol.* 12: 775346.
25. Kurup, S. P., and R. L. Tarleton. 2014. The *Trypanosoma cruzi flagellum* is discarded via asymmetric cell division following invasion and provides early targets for protective CD8$^+$ T cells. *Cell Host Microbe* 16: 439–449.
26. Motwani, M., S. Pesiridis, and K. A. Fitzgerald. 2019. DNA sensing by the cGAS–STING pathway in health and disease. *Nat. Rev. Genet.* 20: 657–674.
27. Gui, X., H. Yang, T. Li, X. Tan, P. Shi, M. Li, F. Du, and Z. J. Chen. 2019. Autophagy induction via STING trafficking is a primordial function of the cGAS pathway. *Nature* 567: 262–266.
28. Watson, R. O., S. L. Bell, D. A. MacDuff, J. M. Kimmey, E. J. Diner, J. Olivas, R. E. Vance, C. L. Stallings, H. W. Virgin, and J. S. Cox. 2015. The cytosolic sensor cGAS detects *Mycobacterium tuberculosis* DNA to induce type I interferons and activate autophagy. *Cell Host Microbe* 17: 811–819.
29. Schoggins, J. W., D. A. MacDuff, N. Imanaka, M. D. Gainey, B. Shrestha, J. L. Eitson, K. B. Mar, R. B. Richardson, A. V. Ratushny, V. Litvak, et al. 2014. *Pan*-viral specificity of IFN-induced genes reveals new roles for cGAS in innate immunity. [Published erratum appears in 2015 *Nature* 525: 144.] *Nature* 505: 691–695.
30. Li, X. D., J. Wu, D. Gao, H. Wang, L. Sun, and Z. J. Chen. 2013. Pivotal roles of cGAS-cGAMP signaling in antiviral defense and immune adjuvant effects. *Science* 341: 1390–1394.
31. Ishikawa, H., Z. Ma, and G. N. Barber. 2009. STING regulates intracellular DNA-mediated, type I interferon-dependent innate immunity. *Nature* 461: 788–792.
32. Ni, G., Z. Ma, and B. Damania. 2018. cGAS and STING: at the intersection of DNA and RNA virus-sensing networks. *PLoS Pathog.* 14: e1007148.
33. Marinho, F. V., S. Benmerzoug, S. C. Oliveira, B. Ryffel, and V. F. J. Quesniaux. 2017. The emerging roles of STING in bacterial infections. *Trends Microbiol.* 25: 906–918.
34. Woodward, J. J., A. T. Iavarone, and D. A. Portnoy. 2010. c-di-AMP secreted by intracellular *Listeria monocytogenes* activates a host type I interferon response. *Science* 328: 1703–1705.
35. Hansen, K., T. Prabakaran, A. Laustsen, S. E. Jørgensen, S. H. Rahbæk, S. B. Jensen, R. Nielsen, J. H. Leber, T. Decker, K. A. Horan, et al. 2014. *Listeria monocytogenes* induces IFNβ expression through an IFI16-, cGAS- and STING-dependent pathway. *EMBO J.* 33: 1654–1666.
36. Wang, P., S. Li, Y. Zhao, B. Zhang, Y. Li, S. Liu, H. Du, L. Cao, M. Ou, X. Ye, et al. 2019. The GRA15 protein from *Toxoplasma gondii* enhances host defense responses by activating the interferon stimulator STING. *J. Biol. Chem.* 294: 16494–16508.
37. Hahn, W. O., N. S. Butler, S. E. Lindner, H. M. Akilesh, D. N. Sather, S. H. Kappe, J. A. Hamerman, M. Gale, Jr., W. C. Liles, and M. Pepper. 2018. cGAS-mediated control of blood-stage malaria promotes *Plasmodium*-specific germinal center responses. *JCI Insight* 3: e94142.
38. Sun, Y., and Y. Cheng. 2020. STING or Sting: cGAS–STING-mediated immune response to protozoan parasites. *Trends Parasitol.* 36: 773–784.
39. Chen, M., L. Yao, L. Zhou, P. Yang, W. Zou, L. Xu, S. Li, and H. Peng. 2022. Toxoplasma gondii ROP18$_I$ inhibits host innate immunity through cGAS–STING signaling. *FASEB J.* 36: e22171.
40. Yilmaz, I. C., E. Dunuroglu, I. C. Ayanoglu, E. M. Ipekoglu, M. Yildirim, N. Girginkardesler, Y. Ozbel, S. Toz, A. Ozbilgin, G. Aykut, et al. 2022. *Leishmania* kinetoplast DNA contributes to parasite burden in infected macrophages: critical role of the cGAS–STING-TBK1 signaling pathway in macrophage parasitemia. *Front. Immunol.* 13: 1007070.
41. Canavaci, A. M., J. M. Bustamante, A. M. Padilla, C. M. Perez Brandan, L. J. Simpson, D. Xu, C. L. Boehlke, and R. L. Tarleton. 2010. In vitro and in vivo high-throughput assays for the testing of anti-*Trypanosoma cruzi* compounds. *PLoS Negl. Trop. Dis.* 4: e740.

42. Bustamante, J. M., F. Sanchez-Valdez, A. M. Padilla, B. White, W. Wang, and R. L. Tarleton. 2020. A modified drug regimen clears active and dormant trypanosomes in mouse models of Chagas disease. *Sci. Transl. Med.* 12: eabb7656.
43. Zhang, Y., L. Yeruva, A. Marinov, D. Prantner, P. B. Wyrick, V. Lupashin, and U. M. Nagarajan. 2014. The DNA sensor, cyclic GMP-AMP synthase, is essential for induction of IFN-β during *Chlamydia trachomatis* infection. *J. Immunol.* 193: 2394–2404.
44. Sun, L., J. Wu, F. Du, X. Chen, and Z. J. Chen. 2013. Cyclic GMP-AMP synthase is a cytosolic DNA sensor that activates the type I interferon pathway. *Science* 339: 786–791.
45. Celentano, A. M., and S. M. González Cappa. 1993. In vivo macrophage function in experimental infection with *Trypanosoma cruzi* subpopulations. *Acta Trop.* 55: 171–180.
46. Hare, D. N., K. Baid, A. Dvorkin-Gheva, and K. L. Mossman. 2020. Virus-intrinsic differences and heterogeneous IRF3 activation influence IFN-independent antiviral protection. *iScience* 23: 101864.
47. O'Neal, J. T., A. A. Upadhyay, A. Wolabaugh, N. B. Patel, S. E. Bosinger, and M. S. Suthar. 2019. West Nile virus-inclusive single-cell RNA sequencing reveals heterogeneity in the type i interferon response within single cells. *J. Virol.* 93: e01778-18.
48. Drayman, N., P. Patel, L. Vistain, and S. Tay. 2019. HSV-1 single-cell analysis reveals the activation of anti-viral and developmental programs in distinct subpopulations. *eLife* 8: e46339.
49. Planelles, L., M. C. Thomas, C. Marañón, M. Morell, and M. C. López. 2003. Differential CD86 and CD40 co-stimulatory molecules and cytokine expression pattern induced by *Trypanosoma cruzi* in APCs from resistant or susceptible mice. *Clin. Exp. Immunol.* 131: 41–47.
50. Alba Soto, C. D., G. A. Mirkin, M. E. Solana, and S. M. González Cappa. 2003. *Trypanosoma cruzi* infection modulates in vivo expression of major histocompatibility complex class II molecules on antigen-presenting cells and T-cell stimulatory activity of dendritic cells in a strain-dependent manner. *Infect. Immun.* 71: 1194–1199.
51. Van Overtvelt, L., N. Vanderheyde, V. Verhasselt, J. Ismaili, L. De Vos, M. Goldman, F. Willems, and B. Vray. 1999. *Trypanosoma cruzi* infects human dendritic cells and prevents their maturation: inhibition of cytokines, HLA-DR, and costimulatory molecules. *Infect. Immun.* 67: 4033–4040.
52. Schoggins, J. W., and C. M. Rice. 2011. Interferon-stimulated genes and their antiviral effector functions. *Curr. Opin. Virol.* 1: 519–525.
53. Martin, D. L., K. Murali-Krishna, and R. L. Tarleton. 2010. Generation of *Trypanosoma cruzi*-specific CD8+ T-cell immunity is unaffected by the absence of type I interferon signaling. *Infect. Immun.* 78: 3154–3159.
54. Hokeness, K. L., W. A. Kuziel, C. A. Biron, and T. P. Salazar-Mather. 2005. Monocyte chemoattractant protein-1 and CCR2 interactions are required for IFN-alpha/beta-induced inflammatory responses and antiviral defense in liver. *J. Immunol.* 174: 1549–1556.
55. Mack, M., J. Cihak, C. Simonis, B. Luckow, A. E. Proudfoot, J. Plachý, H. Brühl, M. Frink, H. J. Anders, V. Vielhauer, et al. 2001. Expression and characterization of the chemokine receptors CCR2 and CCR5 in mice. *J. Immunol.* 166: 4697–4704.
56. Mayadas, T. N., X. Cullere, and C. A. Lowell. 2014. The multifaceted functions of neutrophils. *Annu. Rev. Pathol.* 9: 181–218.
57. Zhang, L., and R. L. Tarleton. 1999. Parasite persistence correlates with disease severity and localization in chronic Chagas' disease. *J. Infect. Dis.* 180: 480–486.
58. Jones, E. M., D. G. Colley, S. Tostes, E. R. Lopes, C. L. Vnencak-Jones, and T. L. McCurley. 1993. Amplification of a *Trypanosoma cruzi* DNA sequence from inflammatory lesions in human chagasic cardiomyopathy. *Am. J. Trop. Med. Hyg.* 48: 348–357.
59. Higuchi, M. L., T. De Brito, M. Martins Reis, A. Barbosa, G. Bellotti, A. C. Pereira-Barreto, and F. Pileggi. 1993. Correlation between *Trypanosoma cruzi* parasitism and myocardial inflammatory infiltrate in human chronic chagasic myocarditis: Light microscopy and immunohistochemical findings. *Cardiovasc. Pathol.* 2: 101–106.
60. Uhlén, M., L. Fagerberg, B. M. Hallström, C. Lindskog, P. Oksvold, A. Mardinoglu, Å. Sivertsson, C. Kampf, E. Sjöstedt, A. Asplund, et al. 2015. Tissue-based map of the human proteome. *Science* 347: 1260419.
61. Poncini, C. V., C. D. Alba Soto, E. Batalla, M. E. Solana, and S. M. González Cappa. 2008. *Trypanosoma cruzi* induces regulatory dendritic cells in vitro. *Infect. Immun.* 76: 2633–2641.
62. Panas, M. W., and J. C. Boothroyd. 2021. Seizing control: how dense granule effector proteins enable *Toxoplasma* to take charge. *Mol. Microbiol.* 115: 466–477.
63. Kurup, S. P., and R. L. Tarleton. 2013. Perpetual expression of PAMPs necessary for optimal immune control and clearance of a persistent pathogen. *Nat. Commun.* 4: 2616.
64. Padilla, A. M., L. J. Simpson, and R. L. Tarleton. 2009. Insufficient TLR activation contributes to the slow development of CD8+ T cell responses in *Trypanosoma cruzi* infection. *J. Immunol.* 183: 1245–1252.
65. Marin-Neto, J. A., E. Cunha-Neto, B. C. Maciel, and M. V. Simões. 2007. Pathogenesis of chronic Chagas heart disease. *Circulation* 115: 1109–1123.
66. Añez, N., H. Carrasco, H. Parada, G. Crisante, A. Rojas, C. Fuenmayor, N. Gonzalez, G. Percoco, R. Borges, P. Guevara, and J. L. Ramirez. 1999. Myocardial parasite persistence in chronic chagasic patients. *Am. J. Trop. Med. Hyg.* 60: 726–732.
67. Marinho, C. R., M. R. D'Império Lima, M. G. Grisotto, and J. M. Alvarez. 1999. Influence of acute-phase parasite load on pathology, parasitism, and activation of the immune system at the late chronic phase of Chagas' disease. *Infect. Immun.* 67: 308–318.
68. Shikanai-Yasuda, M. A., and N. B. Carvalho. 2012. Oral transmission of Chagas disease. *Clin. Infect. Dis.* 54: 845–852.
69. Rassi, A., Jr., A. Rassi, and J. A. Marin-Neto. 2010. Chagas disease. *Lancet* 375: 1388–1402.
70. Choudhuri, S., and N. J. Garg. 2020. PARP1-cGAS-NF-κB pathway of proinflammatory macrophage activation by extracellular vesicles released during *Trypanosoma cruzi* infection and Chagas disease. *PLoS Pathog.* 16: e1008474.
71. de Oliveira, R. B., L. E. Troncon, R. O. Dantas, and U. G. Menghelli. 1998. Gastrointestinal manifestations of Chagas' disease. *Am. J. Gastroenterol.* 93: 884–889.
72. Bustamante, J. M., B. E. White, G. K. Wilkerson, C. L. Hodo, L. D. Auckland, W. Wang, S. McCain, S. A. Hamer, A. B. Saunders, and R. L. Tarleton. 2023. Frequency variation and dose modification of benznidazole administration for the treatment of *Trypanosoma cruzi* infection in mice, dogs, and nonhuman primates. *Antimicrob. Agents Chemother.* 67: e0013223.
73. Zarember, K. A., and P. J. Godowski. 2002. Tissue expression of human Toll-like receptors and differential regulation of Toll-like receptor mRNAs in leukocytes in response to microbes, their products, and cytokines. *J. Immunol.* 168: 554–561.
74. Chao, W. 2009. Toll-like receptor signaling: a critical modulator of cell survival and ischemic injury in the heart. *Am. J. Physiol. Heart Circ. Physiol.* 296: H1–H12.
75. de Kleijn, D., and G. Pasterkamp. 2003. Toll-like receptors in cardiovascular diseases. *Cardiovasc. Res.* 60: 58–67.